

A Mathematical Model for Epitaxial Semiconductor Crystal Growth from the Vapor Phase on a Masked Substrate

Donald A. French (University of Cincinnati),
John Pelesko (Georgia Institute of Technology)

and

Richard Braun (University of Delaware)

Abstract

Certain materials used in lasers are made by a process called epitaxial semiconductor crystal growth. In this report a mathematical model is developed for this growth process which occurs on a substrate at the junction between a masked region and exposed substrate in a vapor. This new model consists of two partial differential equations; one for the surface dynamics and one for the crystal growth on the exposed substrate. An analysis of the steady state solutions is furnished. Approximate solutions for time-dependent cases are found using two numerical methods. An asymptotic analysis is also carried out to determine transient solution behavior. The undesirable "bump" structure at the mask/substrate junction which has been observed experimentally is present in the solutions found by each method.

Report Contributors: Kirk Brattkus (SMU), Pam Cook (University of Delaware), Seongjai Kim (University of Kentucky), and Andrew Roosen (NIST).

Final Oral Presentation: Andrew Roosen (NIST).

Industry Representative: Michael Mauk (AstroPower, Inc.).

Other Project Participants: Gamze Berensel (University of Delaware), Alistair Fitt (University of Southampton), John King (University of Nottingham), Andrew Lacey (Heriot-Watt University), Danny Petrusek (Caltech/UCLA), and Colin Please (University of Southampton).

1 Introduction

Crystals grown on patterned, masked substrates are used in lasers and detectors. The masked substrates may also be used as a diagnostic tool; the crystals grown in artificial geometries may indicate what would be successful or unsuccessful conditions for producing a desired product. The masked substrates may also be used simply for fundamental understanding of the crystal growth process.

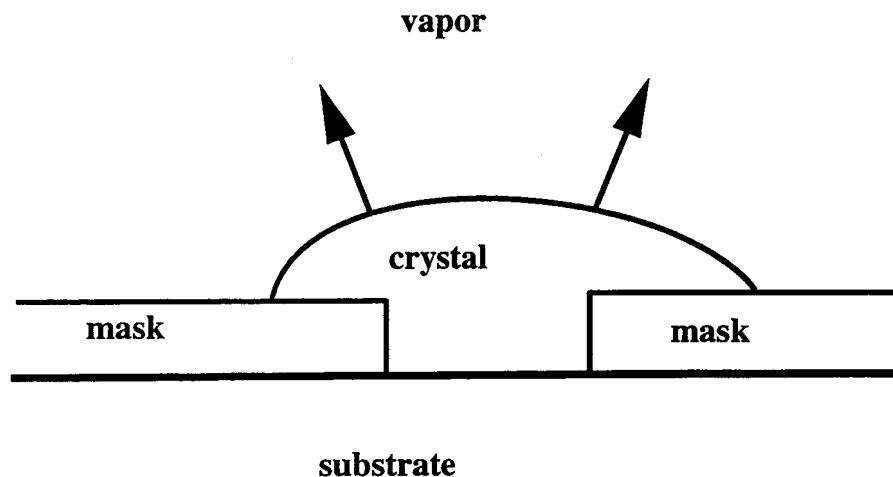


Figure 1: A schematic of epitaxial growth from a masked substrate. Atoms deposited from the vapor accumulate in or near the unmasked region and result in a growing crystal under appropriate conditions. The outward growth is indicated by the arrows.

The growth process that we wish to study is epitaxial crystal growth; epitaxy involves a substrate material such as silicon or other suitable material and the crystal structure and orientation of the substrate is preserved in the growing crystal. The crystal may be grown from particles in a vapor which resides above the surface of the masked substrate. The crystal may also be grown from a very high vacuum process with a beam supplying the material for the crystal; this is molecular beam epitaxy or MBE. The crystal can be grown from the liquid phase as well (liquid phase epitaxy or LPE). We will primarily consider growth from the vapor here. A two-dimensional schematic is shown in Figure 1.

A considerable amount of work has been done on the problem of an unmasked substrate; some recent reviews include [PV, BS, N]. Typically, for electronic applications, one would like to grow a relatively smooth crystal; this will be the case in this work as well. Relatively little work has been done in the case of a partially masked substrate. The thin mask is, in this case, a silicon dioxide film.

A large number of experimental results and associated questions on epitaxial semiconductor crystal growth were brought to the Mathematical Problems in Industry workshop by Michael Mauk of AstroPower, Inc. The working group focused on the specific problem of undesirable crystal growth — the formation of a “bump” — at junctions between the mask and exposed substrate, which are at the perimeter of the crystal. The bumps may appear in growth from the liquid or vapor phases, depending on the material system. In LPE, one would certainly expect bulk diffusion in the liquid to be important, and it may contribute in growth from the vapor.

Geometric growth models based on the kinetic anisotropy have also been developed for highly anisotropic crystals grown from selectively masked substrates [JSLH]. In these models, the growth rate must be known as a function of orientation; from that empirical data, the Wulff shape may be developed that appears to have some success in predicting faceted crystal shapes. Some impressive computations have been carried out using level set methods for geometric growth models of various situations in microchip fabrication ([Se], both with and without anisotropy).

Some previous work in this area suggested that bulk diffusion may be a cause of bumps in some situations [BBK]; the diffusion model for vapor phase epitaxy studied there predicted elevated crystal surfaces near the edge of the mask and a thinner region in the middle of the crystal. That behavior is characteristic of the measured profiles found at AstroPower [M]. The cause of the bump appears to be the "point effect" in the diffusion model of [BBK]. In growth from the vapor, there may be some experimental conditions and/or material systems for which surface diffusion or other surface effects may be important [PV,BS].

It was the intuition of Mauk that the competition of bulk and surface diffusion may be relevant in bump formation. The working group focussed on the role of surface diffusion, sublimation and growth. Continuum models of the surface concentration on the mask and of the crystal surface shape were developed for this purpose. Subsequent models offer the possibility of combining these effects with bulk diffusion to study their competition. One must understand the mathematical problem with surface diffusion alone before letting them both compete.

In this report, a mathematical model consisting of two partial differential equations is formulated for this situation. Both differential equations govern the transport of atoms that will eventually form the growing crystal. One of the equations governs the surface concentration of the atoms on the mask while the other involves the height of the growing crystal on the exposed substrate. Surface diffusion is the main physical phenomenon modeled in the first equation as well as the amount of crystal particles leaving and arriving from the vapor above. The other equation models the motion of the interface between the vapor and the crystal originating above the substrate.

The equations and added physical boundary conditions and initial conditions are nondimensionalized using physical constants obtained from the industry representative's experiments. A parameter ϵ which is the quotient of the diffusion on the crystal over the diffusion on the mask is small. This fact is exploited in an asymptotic analysis of a linearized version of the original problem. A transient "bump" is found in the asymptotic solutions.

A finite difference method is used to find approximate solutions to the nondimensionalized equations. The numerical solutions from both the linearized and nonlinear equations can also exhibit the transient "bump".

The steady state situation is considered and an explicit solution is found. A result of this analysis is the following: a steady state solution exists only if a parameter δ , which is proportional to the surface energy on the crystal divided by the diffusion on the mask, is sufficiently large.

An outline of this report is as follows. In Section 2 we formulate the mathematical model,

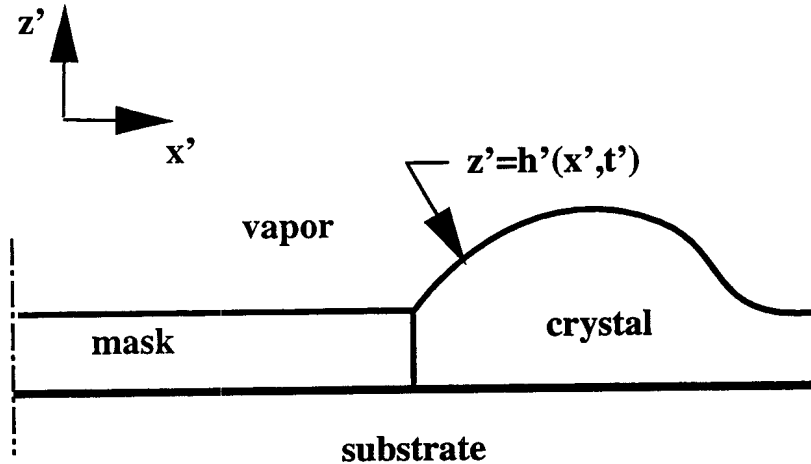


Figure 2: A sketch of the mathematical situation. The free surface of the growing crystal is $z' = h'(x', t')$ in dimensional variables. The free surface is sketched such that a “bump” is shown near the edge of the mask ($x = 0$).

list our physical constants, and provide details of our nondimensionalization. In Section 3 we derive an asymptotic approximate solution. In Section 4 we present the study of the steady state situation and in Section 5 we describe the numerical computations we performed on the nondimensionalized problem. Finally, in Section 6 we give some conclusions and future directions for research beyond the workshop.

2 Mathematical model

In this section we describe the mathematical model which is an initial/boundary value problem consisting of two partial differential equations, one describing the surface concentration of the crystal on the mask and the other involving the motion of the crystal/vapor interface originating from the exposed substrate. We also introduce physical constants and use them to nondimensionalize the problem.

2.1 Surface diffusion over the mask

Our study is on the flat surface covered by the mask material with a periodic series of parallel long trenches where the substrate is exposed. We examine the growth behavior on a partial cross-section which is a line segment extending from the center line of one of the masked “plateaus” to the center of the next trench; a sketch of the mathematical situation is given in Figure 2. We assume the surface behavior is constant in the perpendicular

directions (out of the page) to legitimize this one-dimensional study. Thus we will pose our problem on the interval $-\ell < x' < L$, apply symmetry boundary conditions at $-\ell$ and L , and use an independent variable x' .

The interval $-\ell < x' < 0$ corresponds to the zone where the thin mask is located. Here we study the surface diffusion of the concentration of atoms on the mask, $n_m = n_m(x', t')$;

$$\frac{\partial n_m}{\partial t'} = D_s^{(m)} \frac{\partial^2 n_m}{\partial (x')^2} + J_g - \frac{n_m}{\tau_m}. \quad (1)$$

Here J_g represents the concentration of atoms leaving the vapor and resting on the surface. The term n_m/τ_m provides the concentration of atoms leaving the surface to go into the vapor. The constant τ_m is the mean residence time of atoms. Finally, $D_s^{(m)}$ is the surface conductivity of the crystal concentration on the mask. Note that (1) has been given by [KM] and [N], for example.

Appended to (1) is a symmetry boundary condition,

$$\frac{\partial n_m}{\partial x'}(-\ell, t') = 0. \quad (2)$$

We assume that the atoms close to the substrate will be absorbed quickly; thus we take the boundary condition on the other end of the mask to be a perfect sink:

$$n_m(0, t') = 0. \quad (3)$$

An initial condition is also needed to define this part of the problem completely:

$$n_m(x', 0) = 0. \quad (4)$$

2.2 Model for the crystal surface

We now turn to the formulation of the equation and the associated boundary and initial conditions for the motion of the interface between the crystal that is built-up from the substrate on the interval $0 < x' < L$ and the vapor above. It is possible that this interface can move above the mask on the interval $-\ell < x' < 0$; in this work we assume that this will not occur. This development of the model closely parallels that of Mullins [Mu] in his now classic study of grain boundary grooving.

The interface moves via two mechanisms. The first is from a flux of atoms to the interface from the vapor; this flux is normal to the interface. This contribution to the motion is proportional to the jump in the chemical potential across the interface, viz.,

$$MA(\mu_V^T - \mu_c). \quad (5)$$

Here M is the mobility of the interface and $A = \partial n_s / \partial \mu$ is the change of surface concentration n_s with chemical potential μ ; μ_c is chemical potential of the crystal surface and is given by

$$\mu_c = \mu_\infty + \Omega\gamma\kappa; \quad (6)$$

γ is the surface energy of the crystal, Ω is the atomic volume, κ is the curvature of the crystal surface and μ_∞ is the reference value of the chemical potential for the crystal with a flat surface. μ_V^T is the chemical potential of the vapor and it may be written as $\mu_V^T = \mu_V + \mu_\infty$. The difference between the two chemical potential eliminates the reference value, and successfully indicates that the crystal grows when the chemical potential of the vapor exceeds that of the crystal.

The magnitude of A is estimated very simply by comparing with Mullins [Mu]; comparing our terms with his, one sees that A plays a role identical to n_s/kT , where n_s is the surface concentration, k is Boltzmann's constant, and T is the absolute temperature. Using Mullins' estimate for $n_s \approx 1.5 \times 10^{15}$ atoms/cm² for Ag and our estimate of $T = 1200\text{K}$, we find that $A = n_s/(kT) \approx 10^{28}$. We shall use this estimate in the physical parameters in the next section.

The second contribution is from the surface diffusion of atoms along the interface; the current of atoms J_s is proportional to the gradient of the chemical potential along the surface. For the curve in the plane, the surface gradient is the derivative with respect to arc length, hence

$$J_s = -AD_s^{(c)} \frac{\partial \mu_c}{\partial s'}. \quad (7)$$

The contribution to the rate of increase in the atoms per unit area (proportional to the normal velocity) is proportional to the surface divergence of this flux; for the curve, we have $(-\partial J_s / \partial s')$.

The net rate of increase in the number of atoms per unit area (or the time rate of change of the concentration) may be written as v_n/Ω , where the Ω is the atomic volume and v_n is the normal velocity. Combining the normal and surface diffusion fluxes results in

$$\frac{v_n}{\Omega} = A \left\{ \frac{\partial}{\partial s'} \left[D_s^{(c)} \frac{\partial}{\partial s'} (\Omega \gamma \kappa) \right] + M(\mu_V - \Omega \gamma \kappa) \right\}. \quad (8)$$

If $z' = h'(x', t')$ gives the height of the interface above the substrate, and the curve describing the interface is single-valued, we have the useful relations

$$v_n = \frac{\partial h' / \partial t'}{[1 + (\partial h' / \partial x')^2]^{1/2}} \quad \text{and} \quad \kappa = \frac{-\partial^2 h' / \partial (x')^2}{[1 + (\partial h' / \partial x')^2]^{3/2}}.$$

Note that the units of κ are L^{-1} . By using these expressions, we can write a partial differential equation for the evolution of the free surface of the growing crystal.

At $x' = L$ we assume the symmetry conditions,

$$\frac{\partial h'}{\partial x'}(L, t') = 0 \quad \text{and} \quad \frac{\partial^3 h'}{\partial (x')^3}(L, t') = 0. \quad (9)$$

On the left edge of the substrate, we assume the height of the crystal is the same as that of the mask;

$$h'(0, t') = \bar{h}_0. \quad (10)$$

Table 1: Physical constants.

Constant	Description	Value/Units
J_g	Atoms leaving vapor over mask	9×10^{14} Atoms/(cm ² -sec)
τ_m	Mean residence time of atoms on mask	1 sec
$D_s^{(m)}$	Diffusivity on mask	5×10^{-5} cm ² /sec
$D_s^{(c)}$	Diffusivity on crystal surface	10^{-9} cm ² /sec
L	Length of substrate region	5×10^{-4} cm
ℓ	Length of mask region	5×10^{-4} cm
Ω	Atomic Volume	2×10^{-23} cm ³ /Atom
γ	Surface energy	5×10^3 ergs/cm ²
h_0	Height of mask above substrate	10^{-7} cm
A	Change in concentration/Change in chemical potential	2×10^{28} Atoms ² /(erg-cm ²)
μv	Chemical potential in the vapor	3×10^{-13} erg/atom
M	Mobility	10^1 sec ⁻¹

We also match the fluxes from the atoms on the mask surface moving from left-to-right with the flux onto the growing crystal by requiring that

$$D_s^{(m)} \frac{\partial n_m}{\partial x'}(0, t') = AD_s^{(c)} \Omega \gamma \frac{\partial \kappa}{\partial s'}(0, t') \quad (11)$$

Finally, we assume initially the crystal layer is the same height as the mask; then

$$h'(x', 0) = \bar{h}_0. \quad (12)$$

2.3 Nondimensionalization

To complete this section we now describe the the nondimensionalization used. Table 2 has all the nondimensional parameters.

As above, we first handle the part of the problem defined over the mask. Letting

$$x' = Lx, \quad t' = \frac{L^2}{D_s^{(m)}} t, \quad \text{and} \quad n_m = \tau_m J_g u$$

we can rewrite (1)-(4) as

$$\frac{\partial u}{\partial t} = \frac{\partial^2 u}{\partial x^2} + \alpha(1 - u) \quad (13)$$

with boundary conditions

$$\frac{\partial u}{\partial x}(-d, t) = 0 \quad \text{and} \quad u(0, t) = 0 \quad (14)$$

and an initial condition

$$u(x, 0) = 0. \quad (15)$$

Table 2: Nondimensional parameters.

Constant	Expression	Approximate Value
ϵ	$D_s^{(c)}/D_s^{(m)}$	2×10^{-5}
D	$(\Omega^2 A \gamma)/(L^2)$	10^{-7}
δ	$(M \Omega^2 \gamma A)/D_s^{(m)}$	10^{-7}
α	$L^2/(\tau_m D_s^{(m)})$	10^1
J	$-(\Omega A \mu_V M L)/D_s^{(m)}$	10^{-5}
η_0	h_0/L	2×10^{-4}
β	$(A \Omega \gamma)/(\tau_m J_g L)$	5×10^{-3}
d	ℓ/L	1

To nondimensionalize (8)-(12) we make the following variable changes, again referring to Tables 1 and 2 for the definitions of the constants:

$$h = L\eta \text{ and } \kappa = L^{-1}K.$$

The second part of the problem then becomes

$$(1 + (\partial\eta/\partial x)^2)^{-1/2} \frac{\partial\eta}{\partial t} = \epsilon D \frac{\partial^2 K}{\partial s^2} - \delta K + J \quad (16)$$

where

$$K = \frac{-\partial^2 \eta / \partial x^2}{(1 + (\partial\eta/\partial x)^2)^{3/2}}.$$

We also have the boundary conditions

$$\frac{\partial\eta}{\partial x}(1, t) = 0, \quad \frac{\partial^3 \eta}{\partial x^3}(1, t) = 0, \quad (17)$$

$$\eta(0, t) = \bar{\eta}_0, \quad (18)$$

and

$$\epsilon\beta \frac{\partial K}{\partial s}(0, t) = \frac{\partial u}{\partial x}(0, t) \quad (19)$$

and the initial condition

$$\eta(x, 0) = \bar{\eta}_0. \quad (20)$$

3 Linear theory

As discussed earlier, epitaxial semiconductor crystal growth on masked substrates often leads to the formation of undesirable crystal structures during the growth process. In

particular, a “bump” structure on the crystal which forms above the unmasked region has been observed experimentally.

We begin by studying the surface diffusion over the mask. The small size of ϵ indicates that diffusion is much faster on the mask, and this suggests that the concentration distribution of atoms on the mask will equilibrate very fast compared to the evolution of the crystal. In the first part of this section, we shall develop that equilibrium solution. In the second part of this section, we develop an asymptotic theory which allows us to understand the growth, shape and evolution of these “bumps.”

3.1 Over the mask

Because we have a linear diffusion problem on a fixed domain, we can find an exact solution to the problem for the concentration on the mask. We must solve equations (13) on the interval $-d < x < 0$, subject to the boundary conditions (14) and initial condition (15). The exact solution to the transient problem is

$$u(x, t) = \sum_{n=0}^{\infty} \frac{\alpha_n}{k_n^2 + \alpha} \left[1 - e^{-(k_n^2 + \alpha)t} \right] \sin(k_n x) \quad (21)$$

where

$$k_n = \frac{(2n + 1)\pi}{2d} \quad (22)$$

and the α_n are the Fourier sine coefficients of the forcing term α .

We can also find the steady state solution from the ordinary differential equation in x :

$$u_{xx} - \alpha u = -\alpha.$$

The solution to this equation, subject to the boundary conditions (14) is

$$u_{\text{steady}}(x) = 1 - \cosh(\sqrt{\alpha}x) - \tanh(\sqrt{\alpha}d) \sinh(\sqrt{\alpha}x). \quad (23)$$

An important quantity that is needed in the next section is the derivative of u at the boundary $x = 0$ this quantity is

$$u'_{\text{steady}}(x) = -\sqrt{\alpha} \tanh(\sqrt{\alpha}d). \quad (24)$$

This flux out of the mask will be used as a boundary condition on the asymptotic analysis of the growing crystal in the next section.

3.2 Linear theory for the growing crystal

We begin by linearizing equations (16)-(20), that is, we neglect terms proportional to η_x^2 and study the following linearized system:

$$\frac{\partial \eta}{\partial t} = -\epsilon D \frac{\partial^4 \eta}{\partial x^4} + \delta \frac{\partial^2 \eta}{\partial x^2} + J \quad (25)$$

$$\eta(0, t) = \bar{\eta}_0 \quad (26)$$

$$\frac{\partial^3 \eta}{\partial x^3}(0, t) = -\frac{1}{\epsilon\beta} \frac{\partial u}{\partial x}(0, t) \quad (27)$$

$$\frac{\partial \eta}{\partial x}(1, t) = 0 \quad (28)$$

$$\frac{\partial^3 \eta}{\partial x^3}(1, t) = 0 \quad (29)$$

$$\eta(x, 0) = \bar{\eta}_0. \quad (30)$$

Without loss of generality, we may take $\bar{\eta}_0 = 0$. Further, we assume that the mask region, with scaled adatom density, u , has equilibrated. Hence, we assume that $u_x(0, t)$ is known and constant, and is given by equation (24). We may then write equation (27) as

$$\frac{\partial^3 \eta}{\partial x^3}(0, t) = \frac{q}{\epsilon\beta} \quad (31)$$

where

$$q = \sqrt{\alpha} \tanh(\sqrt{\alpha}d). \quad (32)$$

3.2.1 Linear steady states

Next, we may consider steady-state solutions of our linearized system, equations (25)-(30). Setting time derivatives to zero and solving the resulting linear ordinary differential equation yields:

$$\eta_{\text{steady}}(x) = \eta_0 + \frac{J}{\delta} x \left(1 - \frac{x}{2}\right) - \frac{q}{\epsilon\beta} \left(\frac{\epsilon D}{\delta}\right)^{3/2} \left[\frac{\cosh\left(\sqrt{\frac{\delta}{\epsilon D}}(1-x)\right)}{\sinh\sqrt{\frac{\delta}{\epsilon D}}} - \coth\sqrt{\frac{\delta}{\epsilon D}} \right]. \quad (33)$$

For realistic values of the parameters, as found in Table 2, a sample plot of this solution is shown in Figure 3. We immediately notice two features of such a plot. First, there are no bumps; this suggests that bumps are a transient phenomena and are smoothed as $t \rightarrow \infty$ in the linearized model. Second, there is a boundary layer near $x = 0$ and a parabolic region away from $x = 0$. It is worth noting that the given form of the steady state solution is better than some other forms involving hyperbolic functions because it minimizes problems due to roundoff error.

We also notice that the limit $\delta \rightarrow 0$ is a singular limit of this steady-solution. This suggests that the full nonlinear problem, equations (16)-(20), may not possess a steady-state solution in the limit $\delta \rightarrow 0$. This limit will be explored for the nonlinear problem more fully in Section 4.

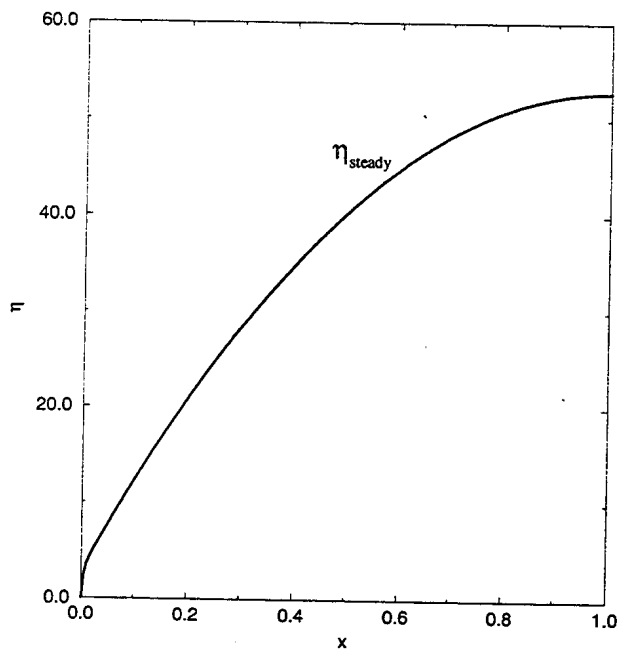


Figure 3: The steady state solution given by Equation (33) for the parameters of Table 2 except that $\bar{\eta}_0 = 0$. The absence of a bump at the left boundary suggests that bumps are a transient phenomenon. Note that there is still a clear transition from a boundary region near $x = 0$ to a more parabolic-looking region away from the boundary.

3.2.2 Transient asymptotic solutions

Now, having identified “bumps” as a transient phenomena, we return to the time dependent linearized problem, equations (25)-(30) and study their evolution. We assume that $\epsilon \ll 1$ and that the remaining parameters scale with ϵ . In particular, we assume that

$$D, \delta, J = O(\epsilon) \quad \beta = O(\sqrt{\epsilon}).$$

Examination of the parameter estimates in Table 2 confirms that this is a physically realistic limit. Suppose we were to seek an asymptotic expansion of the solution in terms of a power series in ϵ :

$$\eta(x, t) \sim \eta_0(x, t) + \epsilon \eta_1(x, t) + \dots \quad (34)$$

Inserting this expansion into equation (25) and equating to zero coefficients of powers of ϵ , we find:

$$\frac{\partial \eta_0}{\partial t} = 0 \quad (35)$$

which immediately implies $\eta_0(x, t) = \eta_0(x)$. Then, by the initial condition, equation (30), we have that $\eta_0 = 0$. Two difficulties with this solution are apparent. First, the boundary condition, equation (27), is not satisfied. That is, the solution is not uniformly valid in space, suggesting the appearance of a spatial boundary layer. Second, if we continue to $O(\epsilon)$, we find:

$$\eta_1(x, t) = (J/\epsilon)t. \quad (36)$$

Recall that from the beginning of the section, J is $O(\epsilon)$, so that J/ϵ is an $O(1)$ quantity. Clearly, the expansion is not uniformly valid in time, which indicates the presence of a temporal boundary layer. This occurs because the ordering of the terms is lost when $t = O(1/\epsilon)$, for example; in that case, the two terms $\eta_0(x, t)$ and $\epsilon \eta_1(x, t)$ are of the same size.

We first patch up the solution on the t time scale by introducing a boundary layer about $x = 0$. Introducing the stretched variable

$$\zeta = \frac{x}{\sqrt{\epsilon}},$$

defining $\beta = \bar{\beta}\sqrt{\epsilon}$, and expanding the solution as before, we find that the leading order inner solution satisfies:

$$\frac{\partial \eta}{\partial t} = -c \frac{\partial^4 \eta}{\partial \zeta^4} + \lambda \frac{\partial^2 \eta}{\partial \zeta^2} \quad (37)$$

$$\eta(0, t) = 0 \quad (38)$$

$$\frac{\partial^3 \eta}{\partial \zeta^3}(0, t) = \bar{q} \quad (39)$$

$$\eta \rightarrow 0 \quad \text{as} \quad \zeta \rightarrow \infty \quad (40)$$

$$\frac{\partial \eta}{\partial \zeta} \rightarrow 0 \quad \text{as} \quad \zeta \rightarrow \infty \quad (41)$$

$$\eta(\zeta, 0) = 0. \quad (42)$$

We note that here, equations (40)-(41) are matching conditions and

$$\lambda = \frac{\delta}{\epsilon}, \quad c = \frac{D}{\epsilon} \quad \text{and} \quad \bar{q} = \frac{q}{\beta},$$

which implies λ , c and \bar{q} are $O(1)$. It is clear that the solution to this problem grows from zero, due to the influx at $\zeta = 0$, and yet it must decay back to zero as $\zeta \rightarrow \infty$. Hence, the solution to this equation represents the evolution of the bump.

Here, we do not present a full solution to the boundary layer equations. Rather, we proceed with the long time analysis, from which information about bump height and lifetime may be gleaned. We now introduce a stretched time variable, $\tau = \epsilon t$, into equations (25)-(29). Note that equation (30) will not hold for the long time problem, but rather initial conditions will be determined by asymptotic matching. Our long time problem is:

$$\frac{\partial \eta}{\partial \tau} = -\epsilon c \frac{\partial^4 \eta}{\partial x^4} + \lambda \frac{\partial^2 \eta}{\partial x^2} + \frac{J}{\epsilon} \quad (43)$$

$$\eta(0, t) = 0 \quad (44)$$

$$\frac{\partial^3 \eta}{\partial x^3}(0, t) = -\frac{1}{\epsilon \beta} \frac{\partial u}{\partial x}(0, t) \quad (45)$$

$$\frac{\partial \eta}{\partial x}(1, t) = 0 \quad (46)$$

$$\frac{\partial^3 \eta}{\partial x^3}(1, t) = 0. \quad (47)$$

Just as for the short time problem, the solution to the long time problem also exhibits a spatial boundary layer structure. Since the boundary layer variable and the expansions in and out of the layer are as before, we do not repeat the analysis here. Rather, we simply note that our leading order outer problem for the long time equations, (43)-(47), is

$$\frac{\partial \eta}{\partial \tau} = \lambda \frac{\partial^2 \eta}{\partial x^2} + \frac{J}{\epsilon} \quad (48)$$

$$\frac{\partial \eta}{\partial x}(1, \tau) = 0 \quad (49)$$

$$\frac{\partial^3 \eta}{\partial x^3}(1, \tau) = 0 \quad (50)$$

$$\eta(0, \tau) = 0. \quad (51)$$

We note that equation (51) is a matching condition obtained by matching into the short time outer solution and that an additional condition at $x = 0$ is obtained by matching into

the long time inner solution. The leading order inner problem for the long time equations is

$$-c \frac{\partial^4 \eta}{\partial \zeta^4} + \lambda \frac{\partial^2 \eta}{\partial \zeta^2} = 0 \quad (52)$$

$$\eta(0, \tau) = 0 \quad (53)$$

$$\frac{\partial^3 \eta}{\partial \zeta^3}(0, \tau) = Q. \quad (54)$$

Here

$$Q = -\frac{\epsilon^{1/2}}{\beta} \frac{\partial u}{\partial x}(0, t). \quad (55)$$

Additional spatial boundary conditions are obtained by matching as $\zeta \rightarrow \infty$, while an initial condition is obtained by matching as $\tau \rightarrow 0$. Both the inner and outer long time problems are easily solved, matched, and a spatially uniformly valid long time solution may be constructed:

$$\begin{aligned} \eta(x, \tau) = & Q \left(\frac{c}{\lambda}\right)^{3/2} \left[1 - \exp\left(-\sqrt{\frac{\lambda}{c}} \frac{x}{\sqrt{\epsilon}}\right) \right] + \frac{1}{\lambda} \sum_{n=0}^{\infty} \frac{1 - \exp(-\lambda \omega_n^2 \tau)}{\omega_n^2} \sin(\omega_n x) \\ & + \sum_{n=0}^{\infty} Q_n \exp(-\lambda \omega_n^2 \tau) \sin(\omega_n x) \end{aligned} \quad (56)$$

Here

$$\omega_n = \frac{(2n+1)\pi}{2}$$

and the Q_n 's are the Fourier sine coefficients of $-Q(c/\lambda)^{3/2}$. From this solution, we immediately obtain an expression for bump height. In particular, as $\tau \rightarrow 0$, this solution approaches the long time limit of the bump evolution equations, (37)-(42). We obtain

$$\text{Bump Height} = Q \left(\frac{c}{\lambda}\right)^{3/2}. \quad (57)$$

Further, since the outer problem for this long time solution smoothes the bump as $\tau \rightarrow \infty$, we may obtain a crude estimate of bump lifetime:

$$\text{Bump Lifetime} \approx \frac{1}{\lambda}. \quad (58)$$

If we undo the scalings to find the physical scales, we find the following. The time scale for the long time problem is $t_0 = L^2/(\epsilon D_s^{(m)}) = L^2 D_s^{(c)}$; for our choice of parameters, this gives $t_0 = 250$ s. The quantity $\lambda = \delta/\epsilon = 5 \times 10^{-3}$ for our parameters. The prediction of the time scale for the life of the bumps is then $t_0/\lambda = 5 \times 10^4$ s ≈ 14 hours. Experiments at AstroPower [M] over the time scales of 1/2 to 3 hours may show bumps, but the bumps do not appear to die out within that time scale. This lifetime estimate from the asymptotics

appears to be reasonable given this information. We shall return to this point in the numerics of Section 5.1.

The bump height may be computed as well; in nondimensional terms, Eq. (57) yields a height of about 2.8; redimensionalizing with $L = 5\mu\text{m}$ yields about a $14\mu\text{m}$ high bump, according to the linear theory.

4 Nonlinear steady states

The time-dependent linear analysis of the last section predicts the growth and deformation of an initially flat crystal interface through the formation of bumps at the mask edge. The question of whether these bumps are transient or whether they grow to establish a steady ridge may be addressed by considering the steady-state solutions to the nonlinear problem (13-20). We conclude from the work in this section that steady solutions do not exist unless the rate of deposition is sufficiently small, $J \leq J_c$ for a critical constant J_c . Also, none of the steady states have the ‘‘bump’’ shape that we are looking for indicating this phenomenon is a transient effect.

The analysis begins by assuming that the interface is stationary, $v_n = 0$, and that the adatom density along the mask, u , is an equilibrium solution to (13-14). In this case our problem reduces to solving an ordinary differential equation for the curvature as a function of arc length, $K(s)$,

$$\epsilon D \frac{d^2 K}{ds^2} - \delta K + J = 0, \quad (59)$$

with the flux condition

$$\left. \frac{dK}{ds} \right|_{s=0} = -\frac{\sqrt{\alpha}}{\epsilon\beta} \tanh \sqrt{\alpha} d, \quad (60)$$

and a symmetry condition applied at the center of the crystal region where $x = 1$ and $s = L^*$. Here L^* is half the total arc length of the interface. Symmetric solutions to equations (59-60) are easily determined to be

$$K = \frac{J}{\delta} + \frac{\tanh \sqrt{\alpha} d}{\beta} \sqrt{\frac{\alpha D}{\epsilon \delta}} \frac{\cosh \sqrt{\frac{\delta}{\epsilon D}} (L^* - s)}{\sinh \sqrt{\frac{\delta}{\epsilon D}} L^*}. \quad (61)$$

The first point to make about this result is that the steady-state curvature is positive definite; the crystal ‘‘opens downward’’ everywhere. The existence of a stationary bump at the crystal-mask edge requires a steady-state curvature that changes sign and so although it was shown in the previous section that our model predicts that ridges do form during the initial stages of deposition, these ridges must be a transitional phenomena. If a steady state exists, the crystal is strictly convex.

The existence of a steady-state, however, is not guaranteed by (61); one must be able to integrate the equation for curvature to find a single-valued interface η that is symmetric about the mid-channel at $x = 1$. This is not always possible. Consider the experimentally

relevant case where the term $\sqrt{\epsilon D/\delta}$ is small. In this case the curvature is constant up to exponentially small terms everywhere outside a layer in arc length at the mask edge of thickness $\sqrt{\epsilon D/\delta}$, viz.,

$$K \sim \frac{J}{\delta}, \quad \sqrt{\epsilon D/\delta} \rightarrow 0. \quad (62)$$

This boundary layer is similar to that seen in the linear case; examples will be plotted below from numerical results. Away from the mask edge ($x = 0$) the crystal forms a circular arc with radius δ/J . This circular arc region corresponds to the parabolic region away from the mask edge in the steady state from the linear problem.

The circular arc is too small to fill the crystal region if $\delta/J < 1$ and as a result there are *no steady-state solutions* to the nonlinear problem (13-20) for small values of $\sqrt{\epsilon D/\delta}$ if the flux of adatoms onto the surface J is larger than δ . In dimensional terms this becomes a restriction on the chemical potential in the vapor; there are no stationary solutions if

$$\mu_V > \frac{\gamma\Omega}{L}. \quad (63)$$

The effect of the terms in (61) that are negligible as $\sqrt{\epsilon D/\delta} \rightarrow 0$ is to increase the magnitude of the interfacial curvature and these terms put an even tighter restriction on the critical size of the deposition flux. For an arbitrary set of parameters, steady states exist only if $J < J_c < \delta$.

5 Numerical experiments

5.1 Linear Theory

In this section, we will numerically integrate the linearized equations for the case with a fixed, known flux from the mask.

The numerical method used for this purpose is as follows. Centered finite differences were used for the 2nd and 4th order spatial derivatives (see, for example, [AS, S]). One can write for any of the spatial derivatives at the point x_i through 4th order:

$$\begin{aligned} \frac{\partial \eta}{\partial x}(x_i) &\approx \frac{\eta_{i+1} - \eta_{i-1}}{2\Delta x}, \\ \frac{\partial^2 \eta}{\partial x^2}(x_i) &\approx \frac{\eta_{i-1} - 2\eta_i + \eta_{i+1}}{(\Delta x)^2}, \\ \frac{\partial^3 \eta}{\partial x^3}(x_i) &\approx \frac{-\eta_{i-2} + 2\eta_{i-1} - 2\eta_{i+1} + \eta_{i+2}}{2(\Delta x)^3}, \\ \frac{\partial^4 \eta}{\partial x^4}(x_i) &\approx \frac{\eta_{i-2} - 4\eta_{i-1} + 6\eta_i - 4\eta_{i+1} + \eta_{i+2}}{(\Delta x)^4}. \end{aligned} \quad (64)$$

These approximations have second-order accuracy, i.e., the truncation error is $\mathcal{O}((\Delta x)^2)$. If these approximations are used while the time variable was left continuous, there results in a system of ODE's to be solved on the uniformly spaced grid points $x_j = j\Delta x$

with $j = 0, 1, \dots, N$ and spacing Δx . The ODE's are solved by the package DASSL [BCP]; the package is in FORTRAN as was the calling program (The code is available via <http://www.math.udel.edu/~braun/download/linearxtal.tar>). DASSL uses a variable time step and variable order Backward Differentiation Formula (or BDF) method which has excellent stability characteristics for stiff problems such as ours [A]. This method is an implementation of the method of lines using finite differences in space and a BDF method in time.

Some care must be taken at the boundary $x = 0$. A modified finite difference formula is used that takes into account that $\eta(0, t) = \eta_0$ is given and that $\eta_{xxx} = q/(\epsilon\beta)$ is given. The formula for the 4th derivative at x_1 is given by

$$\eta_{xxxx}(x_1, t) \approx \frac{2(\eta_1 - \eta_2) + (2/3)(\eta_3 - \eta_0)}{(\Delta x)^4} - \frac{2}{\Delta x} \frac{q}{\epsilon\beta} \quad (65)$$

One way to obtain this equation is to apply a non-centered difference approximation to $\eta_{xxx}(0, t)$ and solve for η_{-1} ; this expression is then used to eliminate η_{-1} in a centered finite difference formula for $\eta_{xxxx}(x_1, t)$.

5.2 Results

Several cases will be examined. First consider the case for the nonlinear results to follow; they are used in the problem specified by Eq. (18); call these conditions Case I. In that case, the parameters are given by $\alpha = 0.2$, $\beta = 0.1$, $\epsilon = 10^{-3}$, $\delta = 10^{-6}$, $J = 10^{-6}$, and $D = 10^{-8}$. We find the results given in Figure 4. The bump can clearly be seen, but the scaling of the asymptotic analysis is not strictly adhered to. The amplitude of the bump from the scalings should be about 10^{-2} , but the numerics give more like 10^{-3} . The lifetime of the bump is around 10^4 ; the time scale of 10^3 for the decay is within an order of magnitude. This is reasonable.

Case II is the parameters $\epsilon = 2 \times 10^{-5}$, $D = 10^{-7}$, $J = 10^{-5}$, $\delta = 10^{-7}$ and $\eta_{xxx}(0, t) = q/(\epsilon\beta) = 300$. Note that these are the values given in Table 2, except that we should have $q/(\epsilon\beta) \approx 3 \times 10^7$. In this case, we are solving Eq. (43), that is, the long-time problem. The initial condition for cases II through V is

$$\eta(x, 0) = 2.5 \times 10^{-4} [1 - \tanh(10x)]. \quad (66)$$

The lifetime of the bump is somewhat shorter than what would be expected of from the asymptotic theory; this is acceptable because the flux boundary condition is not in the asymptotic regime.

Case III is the parameters $\epsilon = 2 \times 10^{-5}$, $D = 10^{-7}$, $J = 10^{-5}$, $\delta = 10^{-7}$ and $\eta_{xxx}(0, t) = q/(\epsilon\beta) = 3 \times 10^5$. In this case, we are again solving Eq. (43), the long-time problem. The size of the bump is about 10 times the thickness of the flat part of the film for a time interval surrounding $\tau = 0.05$. This appears to be consistent with the asymptotic theory. The lifetime of the bump is expected to be on the scale of unity for this choice of parameters.

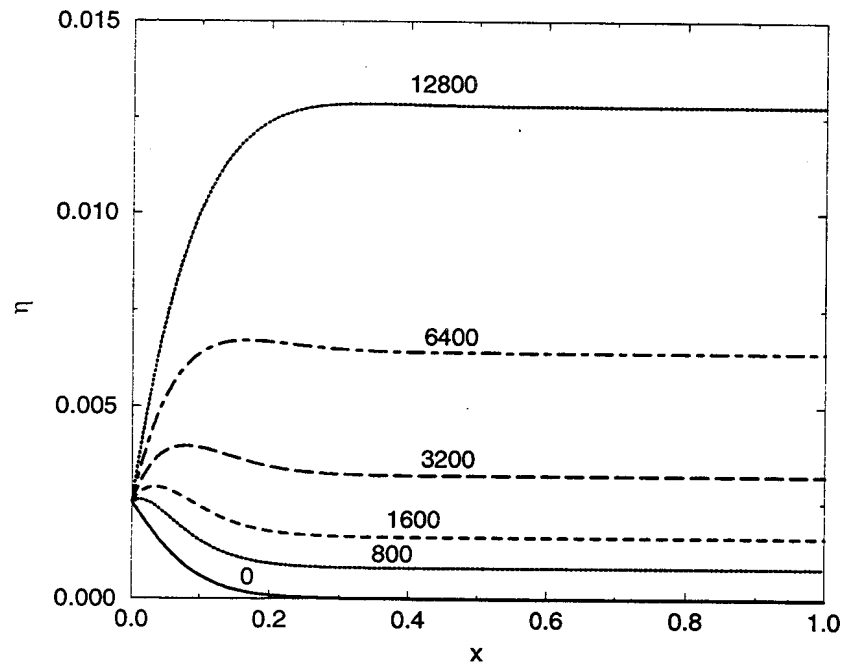


Figure 4: Numerical solution of linearized problem with $\epsilon = 10^{-3}$, $D = 10^{-8}$, $J = 10^{-6}$, $\delta = 10^{-6}$ and $\eta_{xxx}(0, t) = 200$; this is Case I. The solution shows a bump, but the flux at the left end is somewhat less than that given by the nondimensional parameters of Table 2.

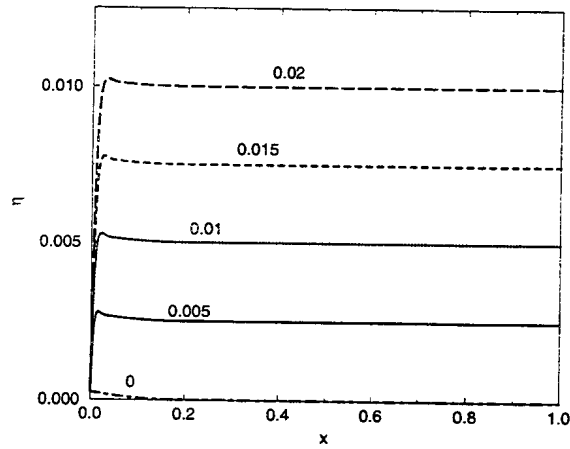


Figure 5: Numerical solution of linearized problem for the parameters of Case II. Values of the nondimensional time τ are indicated near the curves. The solution shows a bump, and the flux at the left end is substantially less than that given by the nondimensional parameters of Table 2.

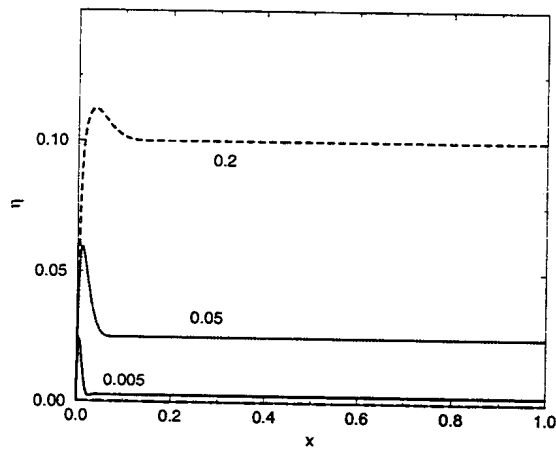


Figure 6: Numerical solution of linearized problem for the parameters of Case III. Values of the nondimensional time τ are indicated near the curves. The solution shows a bump, and the flux at the left end is close to that given by the nondimensional parameters of Table 2.

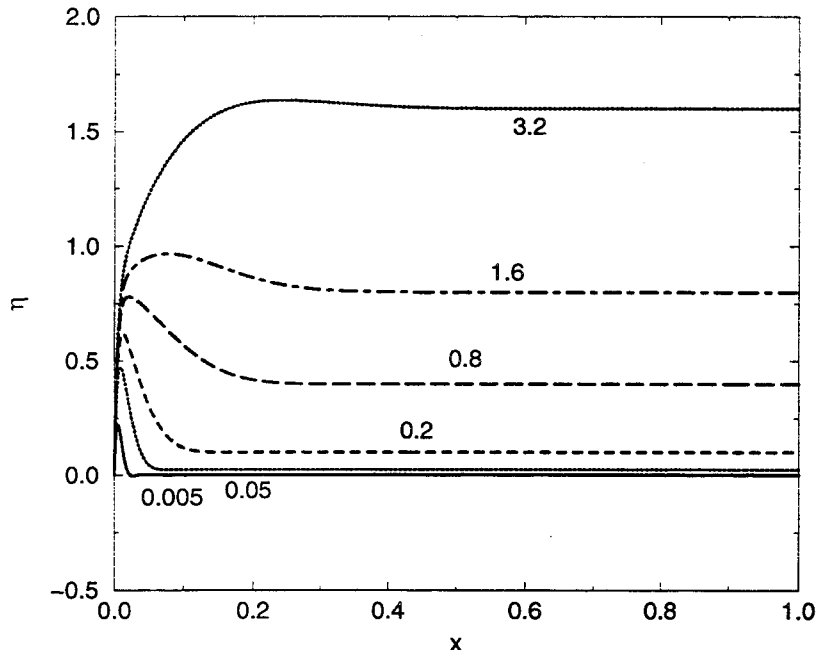


Figure 7: Numerical solution of linearized problem for the parameters of Case IV. Values of the nondimensional time τ are indicated near the curves. The solution shows a bump, and the flux at the left end is close to that given by the nondimensional parameters of Table 2.

For this run, where the flux in from the mask is near the asymptotic regime, we have a timescale for the bump lifetime of about 10^{-1} .

Case IV is the parameters $\epsilon = 2 \times 10^{-5}$, $D = 10^{-7}$, $J = 10^{-5}$, $\delta = 10^{-7}$ and $\eta_{xxx}(0, t) = q/(\epsilon\beta) = 3 \times 10^6$. In this case, we are again solving Eq. (43), the long-time problem, and the flux from the mask is basically in the asymptotic regime. If one takes a close look at the curve for $\tau = 0.005$, one can see that η takes on negative values in a small spatial interval. This is clearly not physical; however, we can observe reasonable later time behavior if we overlook this part of the evolution. The size of the bump is about 10 times the thickness of the flat part of the film for a time interval of roughly $0.05 \leq \tau \leq 0.5$. This appears to be consistent with the asymptotic theory in that the evolution of the bump on the τ time scale for this choice of parameters. Save for initial transients which may be due to a poor choice of initial conditions, the long time behavior of the bumps appears to be captured by the asymptotic theory.

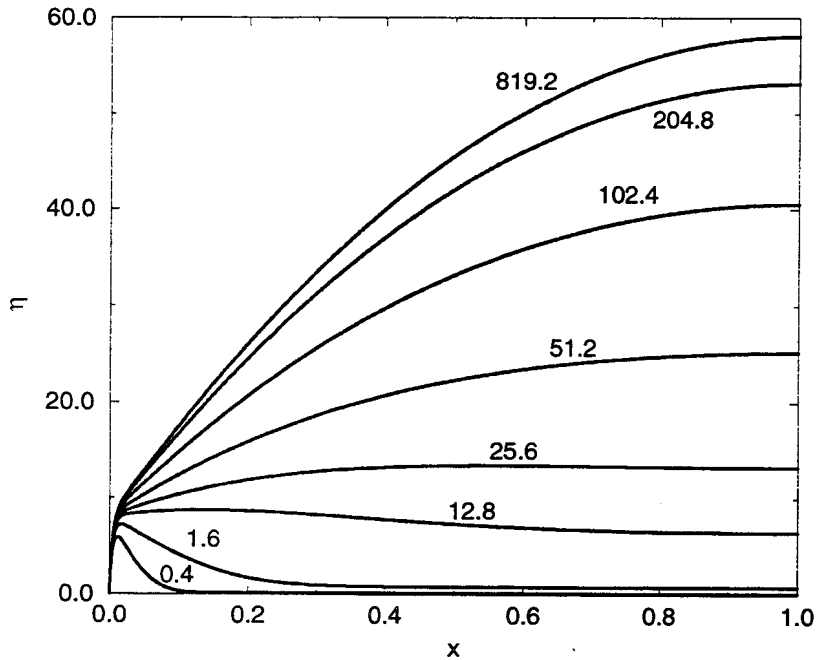


Figure 8: Numerical solution of linearized problem given by Eq. (43) for the parameters of Case V. Values of the nondimensional time τ are indicated near the curves. The solution shows a bump, and the flux at the left end is that of Table 2.

If all of the same parameters are as in Table 2 and we use $q/(\epsilon\beta) \approx 3 = 10^7$, we have Case V. We find oscillations in the interface shape η . This suggests that the η_{xx} is not playing a significant role in the early part of the evolution. We may integrate to long times for Eq. (43), if we ignore the early oscillations. Some results are shown in Figure 8. In the figure, a bump forms near $x = 0$, then evolves to an approximation to the steady state. The solution does not change after $\tau = 819.2$. The solutions show a bump until a time not long after $\tau = 25.6$; this suggests that the bump lifetime, according to these numerics is about 25×250 s or about 1.75 hours. This is about the length of time of the AstroPower experiments, yet they don't see the bumps die out by about twice that time.

Some observations may shed some light on the situation. First, the asymptotics appear to overestimate the lifetime of the bump compared to numerical solutions. The $1/\lambda$ scale is for the decay of the transient solutions to the steady state; this scale fits the evolution shown in Figure 8. Second, the numerics really require better accuracy; inspection of the steady state solution in Eq. (33) compared with the solution at $\tau = 819.2$ in Figure 8 reveals that

the numerics are giving a bigger steady state answer than the exact solution. We presume this is due to the accumulation of numerical error during the evolution. It is worth noting that even evaluating the steady state solution can be difficult numerically; using a formula involving a different combination of the hyperbolic functions results in disastrous roundoff problems. Finally, we are clearly outside of the validity of the linearization of the original equations after just a few time units; the conclusions reached are qualitative for this reason.

It is interesting to note that we can illustrate the balances used in the long time problems given by Eqs. (48)-(51) and (52)-(55) by using numerical results. The absolute value of the terms with with fourth and second order derivatives are plotted in Figure 9, for the data of Case V. The figure shows that the spatial derivative terms are large and that they are the same size in the boundary layer region near $x = 0$. Away from the origin and later in time, the second derivative term is much larger than the fourth derivative term and evolves to about the same size the source term J/ϵ . The second derivative term and the source term

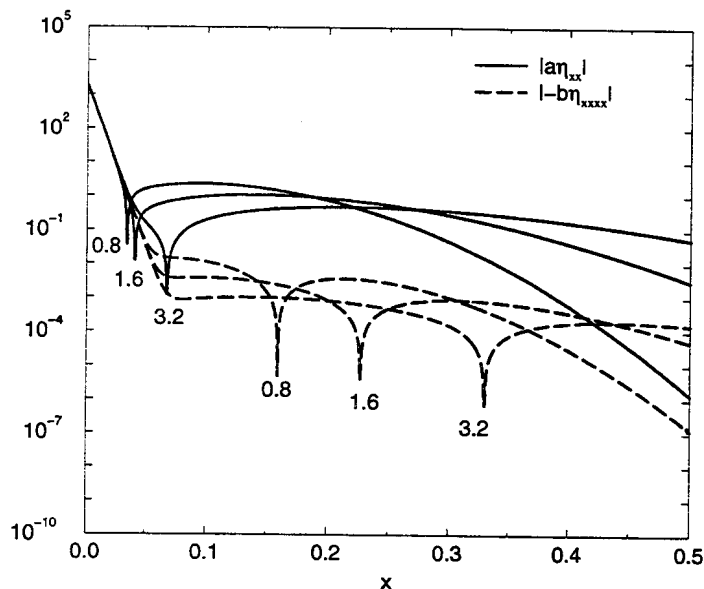


Figure 9: Absolute values of the spatial derivative terms from Eq. (43) for the parameters of Case V at several times. Values of the nondimensional time τ are indicated near the curves. In the figure $b = \epsilon c$ and $a = \lambda$. The different balances seen in the figure justify the scalings used in the long time problems.

J/ϵ are practically identical for the the steady state solution outside of the boundary layer. We now study the nonlinear case.

5.3 Nonlinear Theory

In this section we describe the numerical schemes we have implemented to obtain approximate solutions to (13)-(20). (The code for this section is available via anonymous ftp from <http://www.ms.uky.edu/~skim/download/Crystal.CF.tar>.) Let $T > 0$ be the maximum time for the simulation, the timestep $\Delta t = T/N_t$ for a positive integer N_t , and

$$t^k = k\Delta t, \quad k = 0, 1, \dots, N_t.$$

For the spatial discretization, choose the grid points

$$x_i = i\Delta x, \quad i = 0, 1, \dots, N_x,$$

where $\Delta x = 1/N_x$ for an integer $N_x > 0$. We denote $\eta^k = \eta(\cdot, t^k)$.

Let us begin with the time-stepping procedure for (16). We employ the backward Euler method with the nonlinear terms in (16) treated by the second-order extrapolation: for $k = 0, 1, \dots, N_t - 1$,

$$\phi^{k+1} \frac{\eta^{k+1} - \eta^k}{\Delta t} \approx -\epsilon D \left((\phi^{k+1})^3 \eta_{xx}^{k+1} \right)_{ss} + \delta (\phi^{k+1})^3 \eta_{xx}^{k+1} + J, \quad (67)$$

where

$$\phi^{k+1} = \left(1 + (\partial E \eta^{k+1} / \partial x)^2 \right)^{-1/2}, \quad E \eta^{k+1} = 2\eta^k - \eta^{k-1}. \quad (68)$$

The initial extrapolation is given with the assumption that $\eta \equiv 0$ for $t \leq 0$:

$$E \eta^1 = 2\eta^0 - \eta^{-1} = 0.$$

It is not difficult to see that such an extrapolation approximation has asymptotically the same order of accuracy as fully nonlinear (iterative) schemes; see [D, DDE] for incomplete iterations.

For the spatial discretization, we first replace the surface derivatives by terms including x -derivatives

$$\frac{\partial}{\partial s} \approx \phi^{k+1} \frac{\partial}{\partial x}.$$

Now, it is straightforward to approximate the spatial derivatives by the standard centered differences as described above for spatial derivatives with second order accuracy.

Figures 10-13 show the approximate solutions for η at time $t = 5, 60, 120$, and 180 , respectively. We have chosen $\Delta t = \Delta x = 0.01$. Observe how the ‘‘bump’’ appears and then disappears providing further evidence that it is present but that it is transient.

6 Conclusion

In this report we have described the results of the work performed by the mathematicians who chose to tackle the AstroPower problem. Essentially, the work group identified a particular physical phenomenon to study among many brought by the AstroPower representative,

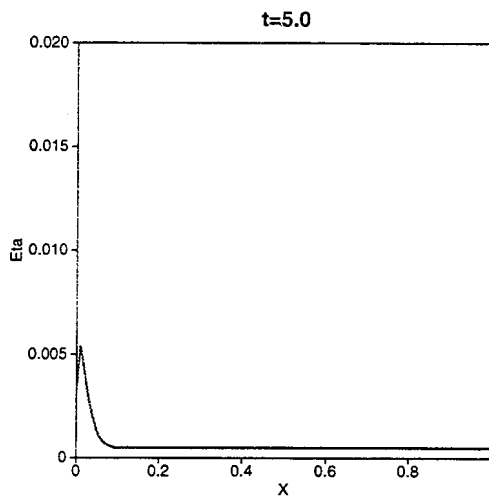


Figure 10: The computed solution η at $t = 5$. The bump appears from an early step.

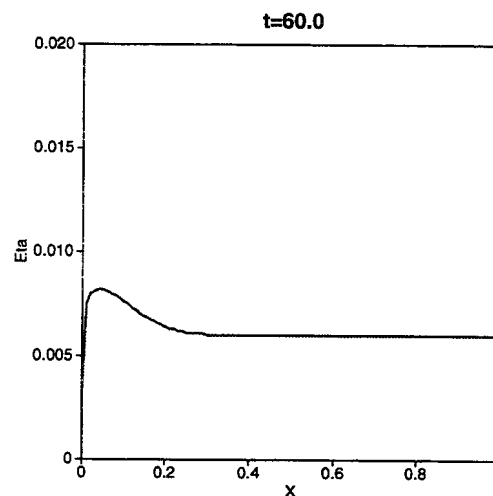


Figure 11: The computed solution η at $t = 60$. One can see the smoothed bump profile due to the surface diffusion between $x = 0.05$ and $x = 0.3$.

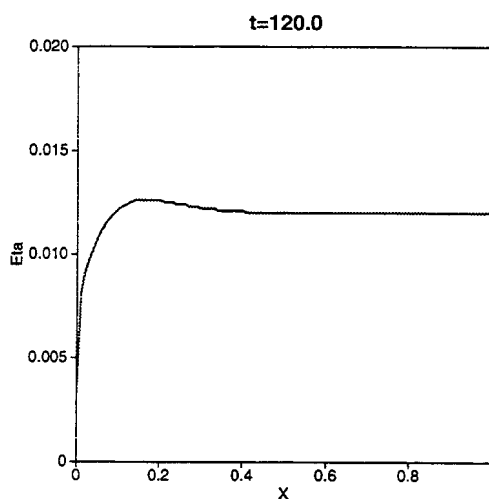


Figure 12: The computed solution η at $t = 120$.

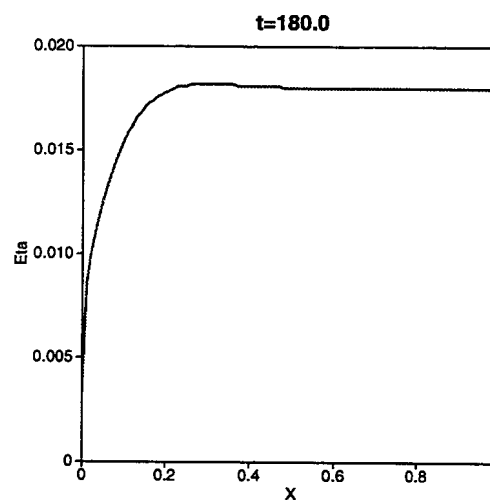


Figure 13: The computed solution η at $t = 180$. Only a trace amount of the bumps remain.

Michael Mauk. The problem chosen involved the undesirable “bump” behavior. A realistic mathematical model was developed. Through the numerical and asymptotic solutions, an understanding and quantification of the formation, behavior, and control of the bump was begun. This model problem suggested new experiments for AstroPower.

Several new research directions were suggested at the workshop which we list, briefly. In experiments it is observed that the crystal growing from the substrate may overgrow onto the mask, and grow outward from the original exposed substrate area. This would give rise to a moving three-phase or contact line in the problem. The presence of three-phase lines may lead to stress singularities in continuum models (see, for example in fluid mechanics, [Da]; with heat transfer, [ADa]; and with evaporation, [ADb]; and references therein). The beginnings of a formulation were attempted, but they were not sufficiently well developed to include in this writeup.

The formulation of the model in terms of dynamic equations for the curvature could be attempted, along the lines of Yokoyama and Sekerka [YS], e.g., and references therein. They find a nonlinear diffusion equation for the curvature of the free surface and then advance the interface with a motion law involving the curvature that specifies the normal velocity of the surface. The difficulties with this formulation are that the boundary conditions may be hard to specify, and that the growth law for the normal velocity of the surface becomes nonlocal.

Anisotropy may be a very important property in the epitaxial semiconductor crystal growth problems because it may have a critical influence on the shape of the growing crystal. To bring this into the current mathematical model we should allow the mobility M , surface diffusion coefficient $D_s^{(c)}$, and the surface energy γ , to depend on the direction of the normal to the free surface; that is, these properties are orientation dependent. These properties could be four-fold or six-fold symmetric depending on the type of crystal grown, but they will generally be four-fold (e.g., for Si).

Other future directions include considering nucleation on the mask, bulk diffusion, and extending the work to two and three dimensional problems. Michael Mauk showed several interesting experiments where the layout of the trenches was crucial to the crystal growth process.

References

- [PV] Alberto Pimpinelli and Jacques Villain, *Physics of Crystal Growth*, (University Press, Cambridge, 1998).
- [BS] A.-L. Barabási and H.E. Stanley, *Fractal Concepts in Surface Growth*, (University Press, Cambridge, 1995).
- [KM] T. Kimoto and H. Matsunami, Surface kinetics of adatoms in vapor phase epitaxial growth on 6H-SiC{0001} vicinal surfaces, *J. Appl. Phys.* **75** (1994), 850-859.

- [N] T. Nishinaga, Nucleation and surface diffusion in molecular beam epitaxy, Chapter 15 in *Handbook of Crystal Growth*, 3 ed. D. T. J. Hurle (1994) Elsevier Science, 666-690.
- [BBK] L.J.M. Bollen, C.H.J. van den Brekel, and H.K. Kuiken, "A mathematical model for selective epitaxial growth," *J. Crystal Growth*, **51** (1981) 581-586.
- [M] Michael Mauk, unpublished research.
- [JSLH] S.H. Jones, L.K. Seidel, K.M. Lau and M. Harold, "Patterned substrate epitaxy surface shapes," *J. Crystal Growth* **108** (1991), 73-88.
- [Se] J.A. Sethian, *Level Set Methods and Fast Marching Methods*, (University Press, Cambridge, 1999, 2nd edition) Chapter 21.
- [Mu] W.W. Mullins, "Theory of thermal grooving," *J. Appl. Phys.* **28** (1957), 333-339.
- [AS] M. Abramowitz and I. Stegun, *Handbook of Special Functions*, (Dover, NY, 1972); see Chapter 25.
- [S] G.D. Smith, *Numerical Solution of Partial Differential Equations: Finite Difference Methods*, (Oxford University Press, Oxford, 1985).
- [BCP] Brennan, K.E., Campbell, S.L., Petzold, L.R., *Numerical Solution of Initial-Value Problems in Differential-Algebraic Systems*, (SIAM, Philadelphia, 1996).
- [A] K. Atkinson, *An Introduction to Numerical Analysis*, (Wiley, NY, 1989, 2nd ed); see Chapter 6.
- [D] J. Douglas, Jr., "On incomplete iteration for implicit parabolic difference equations," *J. Soc. Indust. Appl. Math.* **9** (1961), 433-439.
- [DDE] J. Douglas Jr., T. Dupont, and R.E. Ewing, "Incomplete iteration for time-stepping a Galerkin method for a quasilinear parabolic problem," *SIAM J. Numer. Anal.* **16** (1979), 503-522.
- [Da] S.H. Davis, "Contact line problems in fluid mechanics," *J. Appl. Mech* **50** (1983), 977.
- [ADa] D.M. Anderson and S.H. Davis, "Local fluid and heat flow near contact lines," *J. Fluid Mech.* **268** (1994), 231-265.
- [ADb] D.M. Anderson and S.H. Davis, "The spreading of volatile liquid droplets on heated surfaces," *Phys. Fluids* **7** (1995), 248-265.
- [YS] E. Yokoyama and R.F. Sekerka, *J. Crystal Growth* **125** (1992), 389-403.